Journal of Computational Physics 299 (2015) 472–486

Contents lists available at ScienceDirect

Journal of Computational Physics

www.elsevier.com/locate/jcp

Constrained pressure residual multiscale (CPR-MS) method for fully implicit simulation of multiphase flow in porous media

Matteo Cusini [a,c,*], Alexander A. Lukyanov [b], Jostein Natvig [d], Hadi Hajibeygi [a]

[a] Department of Geoscience and Engineering, Faculty of Civil Engineering and Geosciences, Delft University of Technology, P.O. Box 5048, 2600 GA Delft, The Netherlands
[b] Schlumberger–Doll Research, Cambridge, MA 02139, USA
[c] Politecnico di Milano, Milan, 20100, Italy
[d] SIS Norway Technology Center, Schlumberger, Oslo, 0753, Norway

ARTICLE INFO

Article history:
Received 11 November 2014
Received in revised form 7 July 2015
Accepted 10 July 2015
Available online 15 July 2015

Keywords:
Multiscale methods
Multiscale finite volume method
Multiscale finite element method
Iterative multiscale methods
Algebraic multiscale solver
Scalable linear solvers
Fully implicit simulation
Multiphase flow
Porous media

ABSTRACT

We develop the first multiscale method for fully implicit (FIM) simulations of multiphase flow in porous media, namely CPR-MS method. Built on the FIM Jacobian matrix, the pressure system is obtained by employing a Constrained Pressure Residual (CPR) operator. Multiscale Finite Element (MSFE) and Finite Volume (MSFV) methods are then formulated algebraically to obtain efficient and accurate solutions of this pressure equation. The multiscale prediction stage (first-stage) is coupled with a corrector stage (second-stage) employed on the full system residual. The converged solution is enhanced through outer GMRES iterations preconditioned by these first and second stage operators. While the second-stage FIM stage is solved using a classical iterative solver, the multiscale stage is investigated in full detail. Several choices for fine-scale pre- and post-smoothing along with different choices of coarse-scale solvers are considered for a range of heterogeneous three-dimensional cases with capillarity and three-phase systems. The CPR-MS method is the first of its kind, and extends the applicability of the so-far developed multiscale methods (both MSFE and MSFV) to displacements with strong coupling terms.

1. Introduction

Accurate and efficient numerical simulation of multiphase flow in natural porous media is challenging not only because of highly heterogeneous anisotropic coefficients but also due to the strong flow–transport nonlinear coupling terms. The multiscale finite volume methods (MSFV) [1] have been developed to overcome with the challenge associated with heterogeneous coefficients appearing in the pressure equation. This was achieved by mapping the fine-scale global flow (pressure) equation into a coarse-scale system by using locally computed basis functions [1–4]. The coarse-scale solution is then interpolated (prolonged) back to the original fine-scale resolution, again by using the local basis functions.

The MSFV has been applied to a wide range of applications from compressible and three-phase flows to faults and fractures [5–15]. Its recent advancements involve scalable and conservative iterative strategy which has been benchmarked against the commercial Algebraic MultiGrid (AMG) solvers [16–19]. Note that only a few iterations are required to achieve

* Corresponding author at: Department of Geoscience and Engineering, Faculty of Civil Engineering and Geosciences, Delft University of Technology, P.O. Box 5048, 2600 GA Delft, The Netherlands.
E-mail addresses: m.cusini@tudelft.nl (M. Cusini), ALukyanov@slb.com (A.A. Lukyanov), jnatvig@slb.com (J. Natvig), h.hajibeygi@tudelft.nl (H. Hajibeygi).

http://dx.doi.org/10.1016/j.jcp.2015.07.019
0021-9991/

accurate pressure solutions, used to solve transport equations, because conservative velocity fields can be constructed after any MSFV stage [6,20].

All MSFV methods rely on a sequential (IMPES – or sequential implicit – type) strategy [21] to treat the flow–transport coupling. Unfortunately, when the coupling terms between flow and transport equations are strong, sequential strategies may not be efficient [22]. Strong coupling terms exist in many practical applications, for example in multiphase flows with strong capillary and compositional effects [23,24]. For these cases, fully implicit (FIM) systems are generally more stable than sequential strategies [25,26]. Of great importance in the multiscale community is to develop multiscale methods for fully implicit systems in order to further extend the boundaries of multiscale simulation strategies towards more challenging and realistic cases.

In this work, we devise the first multiscale (MS) method for fully implicit simulations of multiphase flow in highly heterogeneous porous media. Built on the fully implicit Jacobian matrix, a constrained pressure residual (CPR) preconditioning method [27,28] is used to extract the pressure system. This pressure system is then coupled with a second-stage solver for the full residual correction [27,28]. The multiscale solvers are then developed to solve the CPR-based pressure equations leading to a CPR-MS simulation strategy. More precisely, the global solver (for low-frequency errors) is constructed based on a multiscale system (either MSFV or MSFE), before and after which pre- and post-smoothing steps are applied on the fine-scale residual to eliminate high-frequency errors. For solution of the coarse-scale systems the effect of different solution strategies, including AMG [29], is studied.

The performance of CPR-MS for three-dimensional (3D) heterogeneous cases is presented in detail based on CPU times and the number of linear and nonlinear iterations for heterogeneous three-dimensional multiphase flows in presence of gravitational and capillarity effects.

This multistage multiscale strategy (i.e., CPR-MS) combines the advantages of multiscale methods with the stability of fully implicit systems for nonlinear coupled problems. As such, being integrated within the FIM iterative procedure, the CPR-MS captures the strong nonlinear coupling terms and highly heterogeneous coefficients efficiently.

The CPR-MS method is an important advancement that put next-generation multiscale-based reservoir simulators into the context of strong nonlinear physics.

The paper is structured as follows. In Section 2 and Section 3 the CPR-based FIM simulation strategy and the multiscale methods, respectively, are described in brief. Then, the CPR-MS method is presented in Section 4, followed by Section 5, where numerical results are presented for 3D heterogeneous multiphase problems. Finally, the paper is concluded in Section 6.

2. CPR-based fully implicit reservoir simulation

Conservation of mass for multicomponent multiphase fluid flow in porous media using Darcy's law leads to a system of nonlinear coupled equations for N_c components distributed in N_{ph} phases, i.e.,

$$\frac{\partial}{\partial t}\Big(\phi \sum_{j=1}^{N_{ph}} x_{ij}\rho_j S_j\Big) - \nabla\cdot\Big(\sum_{j=1}^{N_{ph}} x_{ij}\rho_j\lambda_j\cdot(\nabla p_j + \rho_j^* g\nabla z)\Big) = q_i, \tag{1}$$

where ϕ is the porosity, x_{ij} is the molar/mass fraction of component i in phase j (N_cN_{ph} unknowns), and S_j (N_{ph} unknowns), p_j (N_{ph} unknowns), ρ_j, ρ_j^*, and λ_j are phase saturation, pressure, molar densities, mass densities, and mobilities, respectively. Gravitational acceleration is denoted by g, which acts in z direction. Moreover, q_i is the i-th component source term.

Equation (1) for N_c components, along with $(N_{ph}-1)$ capillary pressure functions, the saturation constraint $\sum_{j=1}^{N_{ph}} S_j = 1$, N_{ph} phase constraints $\sum_{i=1}^{N_c} x_{ij} = 1$, and $N_c(N_{ph}-1)$ thermodynamic equilibrium equations form a well-posed system of equations to be solved for $N_cN_{ph} + 2N_{ph}$ unknowns [30].

In many cases the behavior of reservoir fluids can be described by the so called black oil model that introduces a three-phase three-component of oil, gas, and water with allowing gas component to appear in (and disappear from) the oil phase through a parameter called solution gas oil ratio, R_s [31]. Equation (1) can be used to describe a black oil system, as a specific example, by introducing the inputs provided in Table 9 of Appendix A.

So far, all multiscale methods have been developed on a sequential simulation strategy. In sequential simulation approach, the system of equations (1) are solved at each time step in two solution steps. First, the component balance equations (either with a volume- or a mass-based approach) are linearly combined to form the pressure equation. This pressure equation is solved first, where only pressure dependent terms are implicitly treated. Then, phase velocities u_j are computed using Darcy's law, i.e., $u_j = -\lambda_j\cdot(\nabla p_j + \rho_j^* g\nabla z)$, and the total velocity is calculated as $u_t = \sum_{j=1}^{N_{ph}} u_j$. The second step includes solving component mass balance equations with using the $\sum_{j=1}^{N_{ph}} S_j = 1$ constraint in order to remove one of the phase saturation unknowns [31,26,7]. Note that all transport dependent terms are fixed when pressure equation is being solved, and all pressure dependent terms are frozen when saturation transport equations are being solved.

It is known that the stability of such an approach is limited to the cases where the coupling between the two equations, i.e., flow (pressure) and transport (saturation), are not strong. Therefore, applicability of this approach for cases with capillarity and compositional effects are questionable [22].

The fully implicit (FIM) approach, however, solves the coupled system of discretized equations for all unknowns simultaneously and implicitly. Therefore, a global linearization method (typically Newton–Raphson) is employed [31], leading to sparse large linear system of equations, i.e.,

$$\mathbf{J}\Delta X = \begin{bmatrix} \mathbf{J}_{pp} & \mathbf{J}_{ps} \\ \mathbf{J}_{sp} & \mathbf{J}_{ss} \end{bmatrix} \begin{bmatrix} \Delta x_p \\ \Delta x_s \end{bmatrix} = r = \begin{bmatrix} r_p \\ r_s \end{bmatrix}, \tag{2}$$

to be solved iteratively until convergence is achieved. Here, the block matrices $\mathbf{J}_{pp}$ and $\mathbf{J}_{ss}$ contain pressure and nonpressure (saturation S_j and component molar fractions x_{ij}) coefficients, respectively. Also, $\mathbf{J}_{sp}$ represents the respective coupling coefficients. Δx_p and Δx_s are the primary (here, pressure) and secondary (here, S_j and x_{ij}) variable increments, respectively. In many practical scenarios, the linear solver step represents a dominant part of the overall computational time. It is a well-known fact that performance of iterative linear solvers strongly depends on robust and fast preconditioners, amenable for massive parallelization. Additionally, for realistic-scale problems, the memory requirement becomes also an important issue.

The CPR method [32,27] was then devised on the basis of targeting the parabolic part of the system (elliptic for incompressible flow) as a separate inner stage (predictor stage), combined with the FIM residual corrector stage. The combination of this predictor–corrector strategy lead to improved convergence properties compared with the case of iterating only on the FIM system.

The CPR pressure equation is extracted from the FIM equation (2). First a decoupling matrix $\mathbf{M}$ is multiplied to the system,

$$\underbrace{\mathbf{MJ}}_{J^*} \Delta X = \underbrace{\mathbf{M}r}_{r^*}, \tag{3}$$

leading to the modified new system $\mathbf{J}^*\Delta X = r^*$, i.e.,

$$\begin{bmatrix} \mathbf{J}^*_{pp} & \mathbf{J}^*_{ps} \\ \mathbf{J}_{sp} & \mathbf{J}_{ss} \end{bmatrix} \begin{bmatrix} \Delta x_p \\ \Delta x_s \end{bmatrix} = \begin{bmatrix} r^*_p \\ r_s \end{bmatrix}. \tag{4}$$

The choices of $\mathbf{M}$ can be made such that the off-diagonal $\mathbf{J}^*_{ps}$ becomes small, or, in the case of Schur complement, it becomes 0. Neglecting $\mathbf{J}^*_{ps}$ can be stated algebraically as multiplying a matrix $\mathbf{C} = [\mathbf{I} \quad \mathbf{0}]^T$ to the system. The pressure system is then formed by solving for an approximate pressure increment $\Delta x'_p$ as

$$\underbrace{(\mathbf{C}^T\mathbf{MJC})}_{\mathbf{A}_{cpr}} \Delta x'_p = \mathbf{C}^T r^*, \tag{5}$$

which is called the CPR pressure system $\mathbf{A}_{cpr} = (\mathbf{C}^T\mathbf{MJC})$.

It is clear that the effectiveness of the CPR procedure depends, to a large extent, on the quality of the extracted pressure matrix $\mathbf{A}_{cpr}$, i.e., the choice of $\mathbf{M}$. Three of the most common options for $\mathbf{M}$ are outlined in the following subsections.

2.1. CPR: ABF reduction approach

In the Alternate-Block Factorization (ABF) procedure [33,34], the decoupling operator is defined as

$$\mathbf{M}^{-1} = \begin{bmatrix} \mathbf{D}_{pp} & \mathbf{D}_{ps} \\ \mathbf{D}_{sp} & \mathbf{D}_{ss} \end{bmatrix} = \begin{bmatrix} \mathrm{diag}(\mathbf{J}_{pp}) & \mathrm{diag}(\mathbf{J}_{ps}) \\ \mathrm{diag}(\mathbf{J}_{sp}) & \mathrm{diag}(\mathbf{J}_{ss}) \end{bmatrix}. \tag{6}$$

Applying this operator to the linear system (2) leads to

$$\mathbf{MJ} = \begin{bmatrix} \Lambda^{-1} & 0 \\ 0 & \Lambda^{-1} \end{bmatrix} \cdot \begin{bmatrix} \mathbf{D}_{ss}\mathbf{J}_{pp} - \mathbf{D}_{ps}\mathbf{J}_{sp} & \mathbf{D}_{ss}\mathbf{J}_{ps} - \mathbf{D}_{ps}\mathbf{J}_{ss} \\ \mathbf{D}_{pp}\mathbf{J}_{sp} - \mathbf{D}_{sp}\mathbf{J}_{pp} & \mathbf{D}_{pp}\mathbf{J}_{ss} - \mathbf{D}_{sp}\mathbf{J}_{ps} \end{bmatrix}, \tag{7}$$

with $\Lambda = \mathbf{D}_{pp}\mathbf{D}_{ss} - \mathbf{D}_{ps}\mathbf{D}_{sp}$. It can be verified that the main diagonal entries of $\mathbf{J}^*_{pp}$ and $\mathbf{J}^*_{ss}$ are all equal to one, and those of the off-diagonal blocks $\mathbf{J}^*_{ps}$, $\mathbf{J}^*_{sp}$ are all equal to zero [34]. Thus, the pressure equation to be solved is

$$\mathbf{J}^*_{pp}\Delta x'_p = \left[\Lambda^{-1}(\mathbf{D}_{ss}\mathbf{J}_{pp} - \mathbf{D}_{ps}\mathbf{J}_{sp})\right] \Delta x'_p = r^*_p. \tag{8}$$

2.2. CPR: quasi-IMPES reduction approach

In the quasi-IMPES approach, the $\mathbf{M}$ matrix reads

$$\mathbf{M} = \begin{bmatrix} \mathbf{I} & -\mathbf{diag}(\mathbf{J_{ps}})\,\mathbf{diag}^{-1}(\mathbf{J_{ss}}) \\ \mathbf{0} & \mathbf{I} \end{bmatrix}, \tag{9}$$

where $\mathrm{diag}(\mathbf{J}_{ps})$ and $\mathrm{diag}(\mathbf{J}_{ss})$ are the diagonal matrices consisting of the main diagonals of $\mathbf{J}_{ps}$ and $\mathbf{J}_{ss}$, respectively.

This choice would then lead to the following pressure equation

$$\mathbf{J}^*_{pp}\ \Delta x'_p = [\mathbf{J}_{pp} \quad -\mathrm{diag}(\mathbf{J}_{ps})\mathrm{diag}^{-1}(\mathbf{J}_{ss})\mathbf{J}_{sp}]\ \Delta x'_p = r^*_p. \tag{10}$$

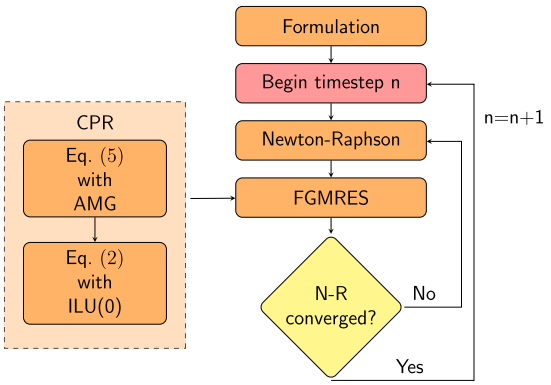

Fig. 1. CPR-based FIM simulation framework: two stage CPR where AMG is used to solve the pressure equation and ILU(0) for the second-stage full residual correction.

2.3. CPR: true-IMPES reduction approach

In the true-IMPES approach, a simplified Schur complement is considered as the decoupling operator, i.e.,

$$\mathbf{M} = \begin{bmatrix} \mathbf{I} & -\text{colsum}(\mathbf{J_{ps}})\ \text{colsum}(\mathbf{J_{ss}})^{-1} \\ \mathbf{0} & \mathbf{I} \end{bmatrix}, \tag{11}$$

where 'colsum' operator replaces $\mathbf{J}_{ps}$ and $\mathbf{J}_{ss}$ matrices by vectors whose elements are the sums of each column. Therefore, the off-diagonal sub-matrix reads

$$\mathbf{J}^*_{ps} = [\mathbf{J}_{ps} - \text{colsum}(\mathbf{J}_{ps})\text{colsum}(\mathbf{J}_{ss})^{-1}\mathbf{J}_{ss}], \tag{12}$$

which is nonzero, but will be eliminated in the pressure equation (by employing operator $\mathbf{C}$). Finally, the pressure equation reads

$$\mathbf{J}^*_{pp}\Delta x'_p = [\mathbf{J}_{pp} - \text{colsum}(\mathbf{J}_{ps})\text{colsum}(\mathbf{J}_{ss})^{-1}\mathbf{J}_{sp}]\Delta x'_p = r^*_p. \tag{13}$$

Equation (5), using one of the three mentioned options for $\mathbf{M}$, forms the first stage of the iterative procedure at each time step. As mentioned before, properties of the pressure matrix $\mathbf{A_{cpr}}$ depend strongly on the choice made for the decoupling operator $\mathbf{M}$. The ABF approach generates a strongly nonsymmetric pressure matrix, compared to the original pressure block $\mathbf{J}_{pp}$, which would have negative impact on AMG methods [34]. IMPES-like CPR methods (quasi-IMPES and true-IMPES) would lead to more symmetric pressure equations (compared with ABF). In particular, true-IMPES would construct the closest to a symmetric system [35].

The linear system (2) is solved using Flexible GMRES (FGMRES) [36,37] with a two-stage preconditioner. In the first preconditioner stage, typically one V-cycle of an AMG method is employed to obtain an approximate solution of Eq. (5). In the second preconditioner stage, a classical iterative solver, e.g., ILU(0) [38], is applied to the FIM system. The entire procedure for one time step is illustrated in Fig. 1 [28,39].

3. Algebraic multiscale solver (AMS)

Pressure equation, arising from CPR stage, can be stated as

$$\mathbf{A}^f p^f = q^f, \tag{14}$$

which is referred to as the fine-scale pressure equation. The subindex "cpr" is omitted for simplicity of the notations, i.e., $\mathbf{A}^f = \mathbf{A_{cpr}}$; and, the superscript f stands for fine-scale. Assuming that the fine-scale solution p^f can be approximated as

$$p^f \approx p' = \mathbf{P}p^c, \tag{15}$$

multiscale methods solve a coarse-scale system for p^c, which is then mapped back into the fine-scale resolution by the use of prolongation (interpolation) operator $\mathbf{P}$. The quality of the approximation depends on the quality of the prolongation operator, which has basis function Φ^k in its k-th column. Basis function Φ^k_j is the local solution of the governing equation, or a modified version of it, with zero RHS, on dual-coarse cells $\tilde{\Omega}_j,\ j \in \{1, \ldots, N_d\}$ (see Fig. 2) which is then assembled as

$$\Phi^k = \sum_{j=1}^{N_d} \Phi^k_j. \tag{16}$$

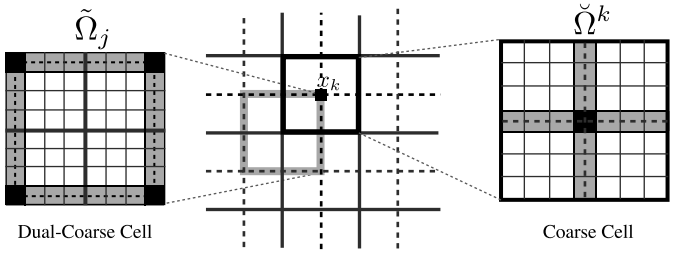

Fig. 2. MSFV grid imposed on the given fine-scale grid (center): N_c coarse (solid lines) and N_d dual-coarse (dashed lines) grids. A coarse and a dual-coarse grid cell are highlighted on the right and left, respectively.

To compute Φ^k, reduced-dimensional boundary condition is employed together with corner values $\Phi^k(x_k) = 1$ and $\Phi^k(x_i) = 0$ at all other coarse nodes (i.e., $\forall i \neq k$) [1,2]. Fig. 2 illustrates the coarse- and dual-coarse grids imposed on the given 2D fine grid. There exist N_c and N_d coarse and dual-coarse grid cells. Note that the coarse cells are required only if an MSFV method is used to solve the coarse-scale system [18].

Starting from the fine-scale system (14), the coarse-scale system is governed by multiplying the restriction operator $\mathbf{R}$ (of dimension $N_c \times N_f$), i.e.

$$\underbrace{(\mathbf{R}\mathbf{A}^f\mathbf{P})}_{A^c} p^c = \underbrace{\mathbf{R}q}_{q^c}, \tag{17}$$

where Eq. (15) is used to replace p^f by p^c. While the prolongation operators for MSFV and MSFE are the same, they employ different restriction operators $\mathbf{R}$. The MSFE uses a classical Galerkin-type operator, i.e., $\mathbf{R_{FE}} = \mathbf{P}^{\mathsf{T}}$. The MSFV, on the other hand, applies a control volume restriction operator $\mathbf{R_{FV}}$, with values in the k-th row being 1 at column j if cell j belongs to the coarse cell k, and 0 elsewhere, i.e.,

$$(\mathbf{R_{FV}})_{kj} = \begin{cases} 1 & \text{if cell } j \in \breve{\Omega}^k, \\ 0 & \text{otherwise.} \end{cases} \tag{18}$$

Although the previously used IMPES pressure discretization differs from that of CPR, it has been successfully employed as a preconditioner for FIM systems [40]. Thus, one may also use the pressure equation of IMPES formulation for the basis function calculations. Another option is to directly employ the CPR-based pressure equation to solve the basis functions. While both approaches are possible, convergence rates and numerical efficiencies can be affected. A comparison study needs to be performed to obtain the optimum formulation for basis functions, similar to [19] for compressible problems, which is beyond the scope of this paper. Next, the AMS solver integrated within a FIM systems (CPR-MS) is described.

4. Constrained pressure residual multiscale (CPR-MS) solver

The CPR-MS algorithm [41] employs a two-stage preconditioner, where an AMS method is used for solving the pressure system extracted by the CPR decoupling operator. Starting from the fully implicit Jacobian matrix $\mathbf{J}$, the solution strategy for one iteration loop is summarized in the following steps:

(1) *Initialize*:
using FIM system solution $x^{*\nu}$, update FIM residual $r^{*\nu}$
(2) *1st stage*: pressure stage
2.1 *CPR stage*: extract $\mathbf{A_{cpr}}$ and r_p^{ν} from the FIM system, as in Eq. (5).
2.2 *Pre-smoothing stage*:
Perform n_{s_1} smoothing iterations on Eq. (5), update accumulated correction vector $\Delta x_p{}^{\nu+s_1} = \sum_{i=1}^{s_1} \Delta x_p'{}^{i}$ and final residual $r_p^{\nu+s_1}$.
2.3 *Employ multiscale stage*:
solve (or iterate on) $\underbrace{(\mathbf{R}\mathbf{A}_{\mathbf{cpr}}\mathbf{P})}_{\mathbf{A}^c} \Delta x_p'{}^{c} = \underbrace{\mathbf{R}r_p^{\nu+s_1}}_{r_p^c}$, and update $\Delta x_p{}^{\nu+s_1+1} = \Delta x_p'{}^{\nu+s_1} + \mathbf{P}\Delta x_p'{}^{c}$ and residual $r_p^{\nu+s_1+1}$.
2.4 *Post-smoothing stage*:
Perform n_{s_2} smoothing iterations on Eq. (5), update $\Delta x_p{}^{\nu+s_1+1+s_2}$ and residual $r_p^{\nu+s_1+1+s_2}$.
(3) *2nd stage*: FIM stage
3.1 *Update the FIM residual*: $r^{*\nu+1} = r^{\nu} - \mathbf{J} \cdot (\mathbf{C} \cdot \Delta x_p{}^{\nu+s_1+1+s_2})$.
3.2 *Employ the second stage preconditioner*: $\Delta x^{*\nu+1} = \mathbf{L}^{-1} \cdot r^{*\nu+1}$.
(4) *Update the solution*: $x^{*\nu+1} = x^{*\nu} + \Delta x^{*\nu+1} + \mathbf{C} \cdot \Delta x_p{}^{\nu+s_1+1+s_2}$.

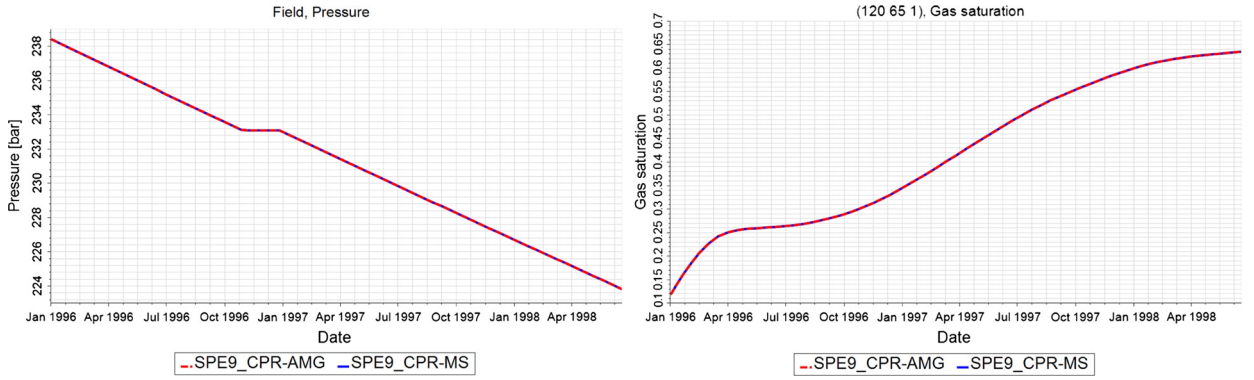

Fig. 3. Field pressure (averaged pressure over the domain) and gas saturation in grid cell (120, 65, 1) for CPR-AMG and CPR-MS, showing that the two solutions match perfectly.

For optimum performance, MS restriction (**R**) and prolongation (**P**) operators (i.e., basis functions) should be adaptively updated based on the local change of parameters [3]. For the test cases of this paper, however, they are computed at the beginning of each time step and kept constant throughout the Newton loop. In addition, the size and sparsity of the coarse pressure matrix depend on the coarsening ratio and the choice of the restriction operator ($\mathbf{R_{FV}}$ and $\mathbf{R_{FE}}$). If the size of the coarse system is small enough, a direct solver can be used. Otherwise, an iterative method should be employed to achieve efficient coarse-scale solutions. Here, different iterative strategies involving AMG are considered.

Finally, Gauss Seidel (GS) and ILU(0) are considered as pre- and post-smoothing steps on the fine-scale pressure system, i.e., Steps (2) and (4). Following [18,19] no Correction Functions neither MSFV coarse-scale solver have been considered in this work.

Next, as a proof of concept, numerical results for three-dimensional heterogeneous problems are presented.

5. Numerical results

Two different heterogeneous three-dimensional models with multiphase flow under gravitational force and injection/production wells are considered: (1) the SPE9 model, (2) the Brill model. The coupling parameters are set such that a sequential strategy encountered difficulties in convergence when capillary effect was considered.

Results and performance were compared with the current version of a modern reservoir simulator which uses CPR preconditioning with True-IMPES decoupling, 1 V-cycle of AMG for solving the CPR pressure system and ILU(0) as a second-stage FIM preconditioner. This reference solution strategy is referred to as CPR-AMG. The coarse grids in AMG solver are constructed by the parallel maximally independent set (PMIS) coarsening scheme with the Gauss–Seidel smoothing process. The coarse level is solved by FGMRES preconditioned by ILU(0) and maximum number of levels is limited to 50 by default settings.

The CPR-MS employs the same decoupling technique and the same second-stage preconditioner, thus, the only difference between CPR-AMG and CPR-MS is the solution strategy for the pressure system. For this reason, all solutions obtained with the CPR-MS and CPR-AMG solvers have been verified to perfectly match each other, as shown, e.g., in Fig. 3.

All results presented were obtained in serial runs using a desktop PC with 20 GB RAM with Intel Xeon X5677 3.47 GHz CPU. The algorithm is highly parallelizable, which is the topic of our ongoing research.

5.1. Black oil SPE9 model

A modified version of the SPE9 model presented in [42] is considered. The original SPE9 grid is refined and a 3-phase (oil, water and gas) black oil case is considered for two scenarios: with and without capillary pressure. The following equilibrium settings are used. Top and bottom of the reservoir are located at 2735.14 m and 3231.52 m, respectively. Datum depth is set at 3032.76 m, and datum pressure is at 3500 psi. The gas–oil contact is located at 3032.76 m, while oil–water contact is located at 3032.76 m. As a result, a two-phase flow is observed. A water injection well and fifteen hydrocarbon productions wells are considered [42]. The fine grid contains $144 \times 150 \times 30$, i.e., 648 000, cells in total, which is a refinement of the original SPE9 model by factor of $6 \times 6 \times 2$ for each cell. Permeability and porosity were copied from coarse cells into fine cells to maintain original geology at the fine scale. The porosity distribution and the permeability field are shown in Fig. 4. With the coarsening ratio of $3 \times 5 \times 5$, the multiscale grid contains $48 \times 30 \times 6$ grid cells, 8640 in total.

This coarsening ratio has been selected as it provided efficient simulations (in terms of CPU) for this model. Note that basis functions are computed using a direct solver, there is no adaptivity applied in their computations, and AMG solver is used to solve the multiscale coarse system. Increasing the coarsening ratio resulted in more computationally expensive basis functions, which without adaptivity would not offset the benefit in convergence properties and thus lead to increased

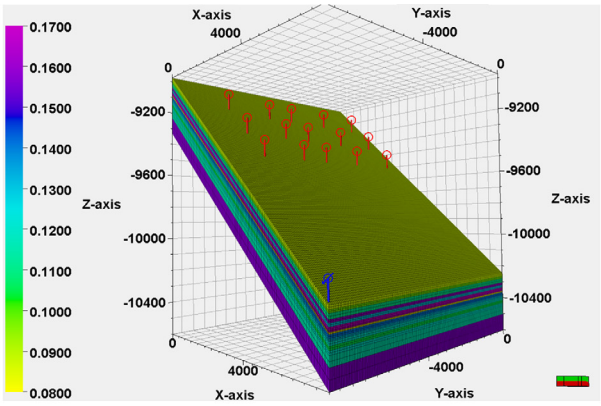

(a) Porosity

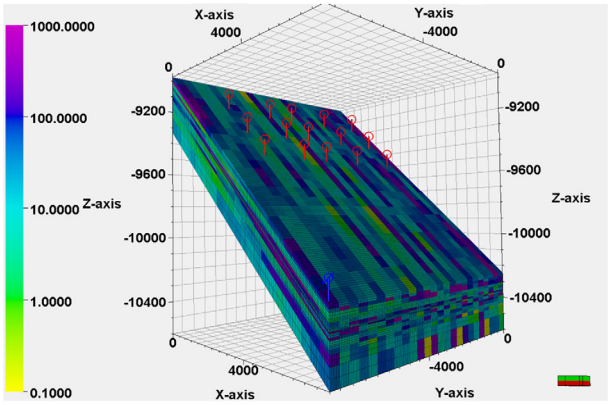

(b) X-Permeability (mD)

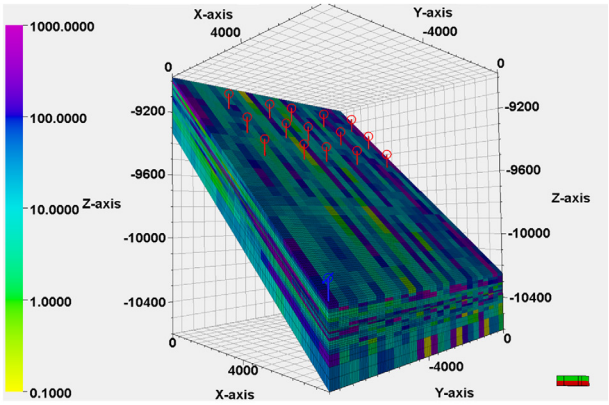

(c) Y-Permeability (mD)

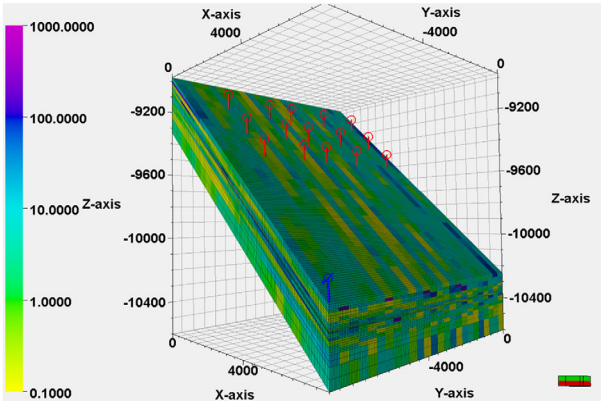

(d) Z-Permeability (mD)

Fig. 4. SPE9 model: porosity and permeability fields. Also shown are the water injection (red) and the hydrocarbon production wells (red). (For interpretation of the references to color in this figure legend, the reader is referred to the web version of this article.)

overall CPU times. Efficient implementation of the CPR-MS including adaptivity based on a rigorous error estimate analysis is a subject of our ongoing research.

The initial conditions of the reservoir are shown in Fig. 5. The FE-based restriction operator was considered, with basis functions which were updated at the beginning of each time-step. Also, the simulation was run for the duration of 900 days.

5.1.1. Simulations without capillary pressure

Table 1 summarizes the settings of the three CPR-MS runs. Two different solvers were used on the coarse pressure system.

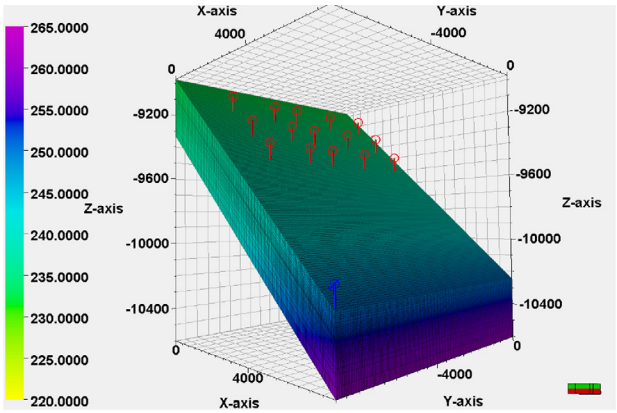

(a) Pressure (bar)

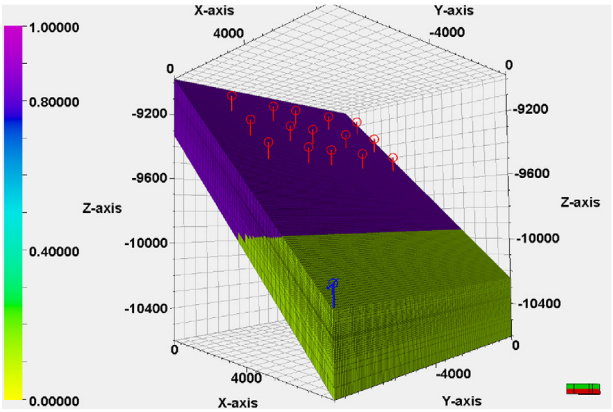

(b) Gas saturation

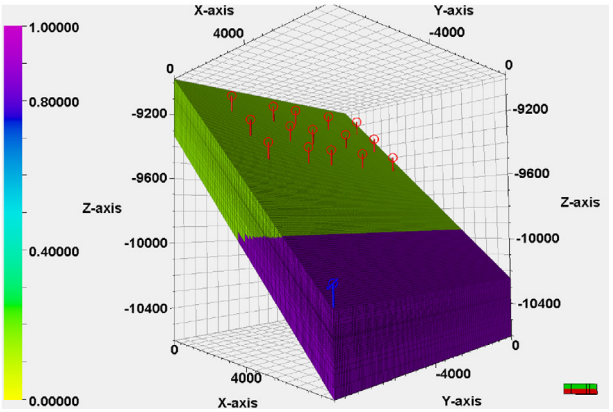

(c) Water saturation

Fig. 5. SPE9 model: pressure, gas and water saturations at the beginning of the simulation. Oil saturation was set to zero for this data set.

Table 1
SPE9 model with capillary pressure: settings. Differences can be seen in the smoothers and in the solver used on the coarse scale pressure system.

Runs	Pre-smoothing	Post-smoothing	Coarse solver
Run 1	GS	GS	AMG
Run 2	GS	GS	GMRES-AMG
Run 3	None	GS	GMRES-AMG

Saturations and pressure maps at the end of simulations are shown in Fig. 6. Table 2 presents the performance of each simulation (number of iterations and CPU time) for the three CPR-MS runs and the CPR-AMG (as the reference) solver.

Note that the number of nonlinear iterations for all 4 runs is the same, meaning that CPR-MS treats the coupling terms as efficiently as CPR-AMG.

Fig. 7 focuses on the linear system CPU time, split into setup and solution phases. The results illustrate the efficiency of the CPR-MS research code developed for this project. Clearly, an adaptive strategy for calculation of the basis functions, and more importantly, implementation of an efficient parallel multiscale algorithm would significantly improve the setup time for CPR-MS. Run 2, which was found as the optimum, involves both pre- and post-smoothing steps with GMRES preconditioned by AMG as the coarse-scale solver.

A breakdown of the CPU time of the CPR-MS pressure solver is presented in Fig. 8. The setup stage of CPR-MS will further improve if an adaptive strategy for basis functions update is employed. Here, the focus is not to find an optimum CPR-MS strategy, but to show fully implicit simulations where AMS is used – for the first time – as the pressure preconditioner. Note that the most time-consuming stages, shown in this figure, are computation of basis functions (dark green bars) and construction of coarse-scale system (**RAP**) (i.e., matrix–matrix multiplications).

The weight of the coarse pressure system solver in the overall CPU time is very small. Comparing Run 2 and 3 for the coarse-system solvers (light green bars in Fig. 8) and the overall performance (i.e., Table 2), the additional costs due to GMRES preconditioned by AMG is offset by the reduction of the overall linear iterations and therefore the overall CPU time.

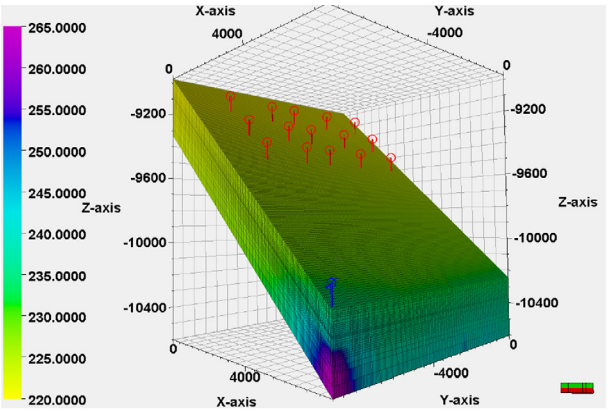

(a) Pressure (bar)

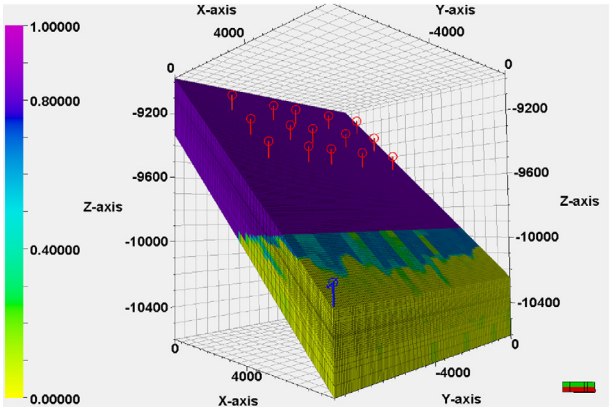

(b) Gas saturation

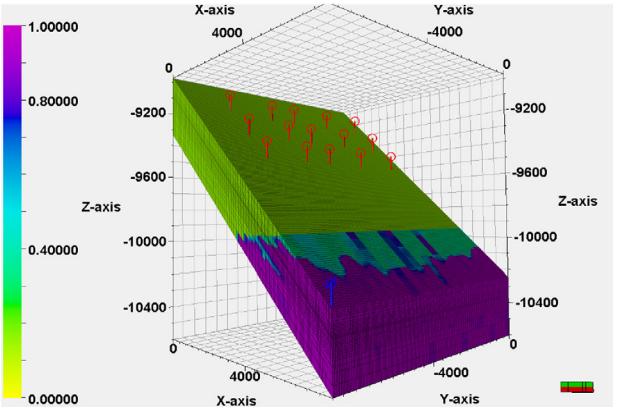

(c) Water saturation

Fig. 6. SPE9 model: pressure, gas and water saturations at the end of the simulation (900th day).

Table 2
SPE9 without capillary pressure: overall performance of the CPR-MS and CPR-AMG.

Runs	Timesteps	Iteration count		CPU time (s)	
		Nonlinear	Linear	Linear solver	Total
Run 1	64	369	2872	1615	2699
Run 2	64	369	2845	1119	2203
Run 3	64	369	3175	1969	3075
CPR-AMG	64	369	2187	1571	2537

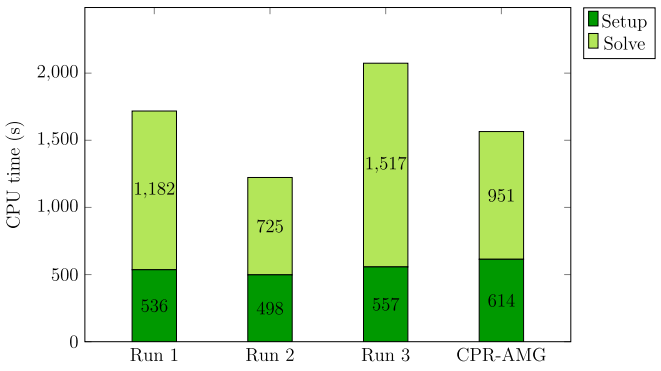

Fig. 7. SPE9 without capillary pressure: LS CPU time (s) breakdown.

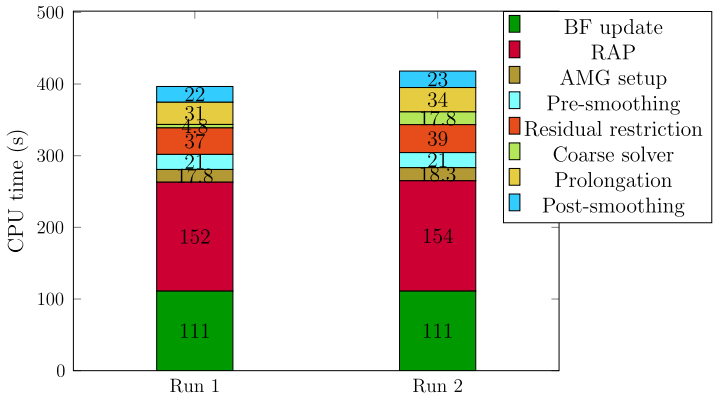

Fig. 8. SPE9 black oil without capillary pressure: pressure solver detailed CPU time breakdown. (For interpretation of the references to color in this figure, the reader is referred to the web version of this article.)

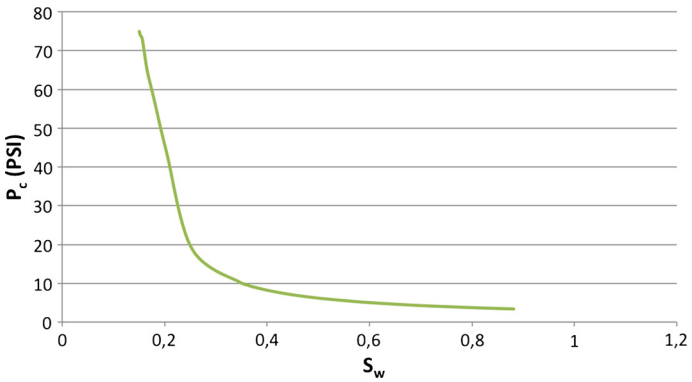

Fig. 9. Capillary pressure curve considered for the case SPE9.

Table 3
SPE9 model with capillary pressure: settings. Differences can be seen in the smoothers and in the solver used on the coarse scale pressure system.

Runs	Pre-smoothing	Post-smoothing	Coarse solver
Run 1	GS	GS	AMG
Run 2	GS	GS	GMRES-AMG
Run 3	2xGS	2xGS	GMRES-AMG

Table 4
SPE9 with capillary pressure: the table shows the total numbers of nonlinear and of linear iterations and the total and the linear solver CPU time of each run.

Runs	Timesteps	Iteration count		CPU time (s)	
		Nonlinear	Linear	Linear solver	Total
Run 1	75	284	1888	759	1672
Run 2	75	284	1867	1202	2130
Run 3	75	281	1627	1105	2036
CPR-AMG	75	281	1381	1093	1863

5.1.2. Simulations with capillary pressure

Keeping the same parameters as in the previous case, the capillary pressure curve (see Fig. 9) is also considered. It is clear that the number of required time steps is increased for all FIM simulators (CPR-MS and CPR-AMG) compared with the previous test case without capillary effects.

Table 3 shows the settings of the different runs that were done with capillary pressure.

Table 4 shows that the CPR-MS and CPR-AMG perform almost the same in terms of the number of time steps and the nonlinear iterations. Note that the performance of CPR-MS, as for the previous case, is influenced by the choice of the coarse pressure solver and the number of smoothing iterations.

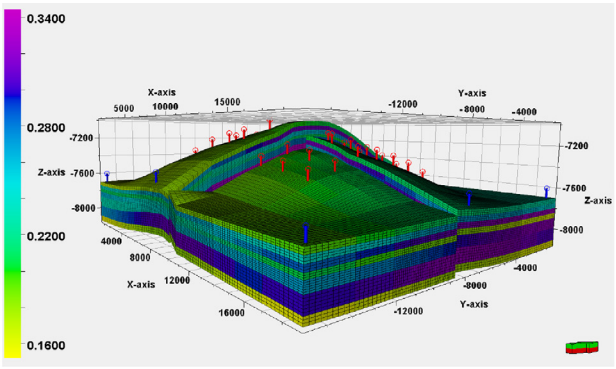

(a) Porosity

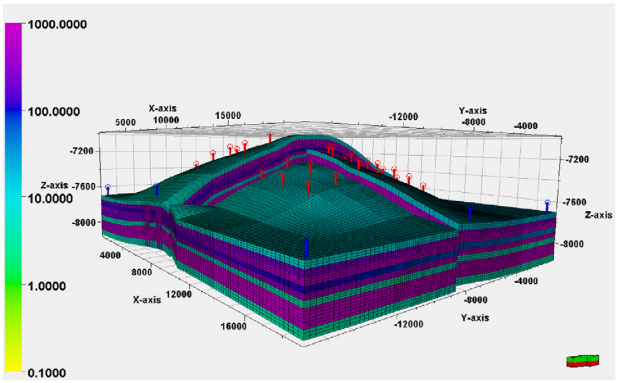

(b) X-Permeability (mD)

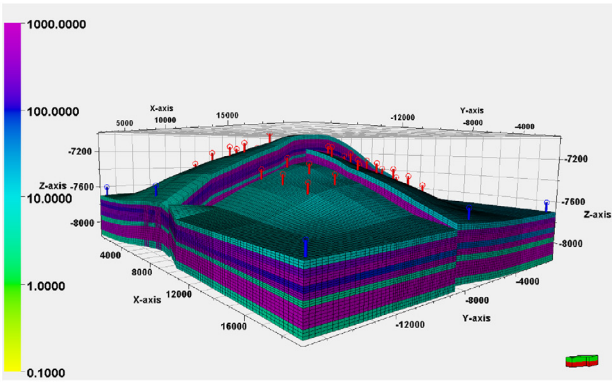

(c) Y-Permeability (mD)

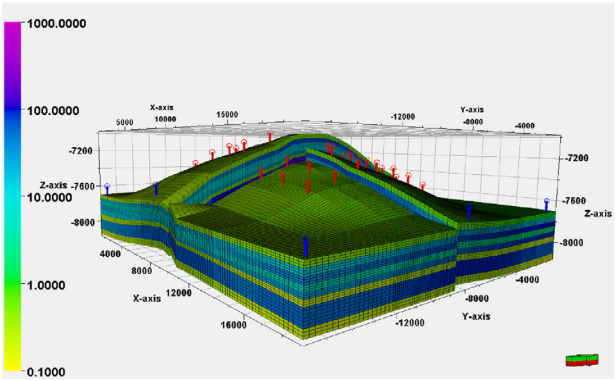

(d) Z-Permeability (mD)

Fig. 10. Brill model: porosity and permeability fields. The injection wells (red) and the production wells (red) are represented. (For interpretation of the references to color in this figure legend, the reader is referred to the web version of this article.)

5.2. Brill model

The Brill model is a 3-phase (water, gas and oil) black oil case that was run both with and without considering capillary pressure. The fine grid contains $180 \times 135 \times 27$, 656 100 in total, cells. There exist 7243 non-neighboring connections in this model. The following equilibrium data has been considered. Top and bottom of the reservoir are located at 2128.57 m and 2490.73 m. Datum depth is located at 2143.05 m, and datum pressure is set at 4500 psi. The gas–oil contact is located at 2143.05 m, while oil–water contact is located at 2438.4 m. As a result, a two-phase flow is observed. The fluid model description can be found in Tables 10 and 11 (see Appendix A), where the Stone three-phase relative permeability for oil phase is used [43].

The porosity distribution and the permeability field are shown in Fig. 10. There exist 8 water injection and 43 hydrocarbon production wells.

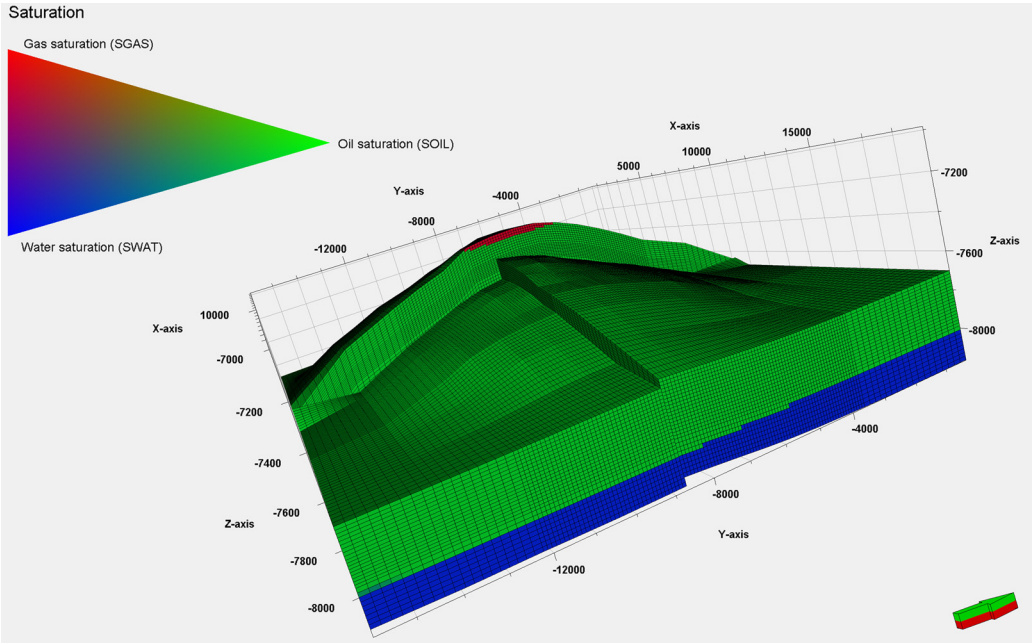

Fig. 11. Brill model: ternary graph of gas (red), oil (green) and water (red) saturations showing the conditions of the reservoir at the beginning of the simulation. (For interpretation of the references to color in this figure legend, the reader is referred to the web version of this article.)

Table 5
Brill model without capillary pressure: settings. Differences can be seen in the smoothers and in the solver used on the coarse scale pressure system.

Runs	Pre-smoothing	Post-smoothing	Coarse solver
Run 1	GS	GS	AMG
Run 2	GS	GS	GMRES-AMG
Run 3	2xGS	2xGS	GMRES-AMG

Table 6
Brill model without capillary pressure: the table shows the total numbers of nonlinear and of linear iterations and the total and the linear solver CPU time of each run.

Runs	Timesteps	Iteration count		CPU time (s)	
		Nonlinear	Linear	Linear solver	Total
Run 1	498	3329	22 201	11 376	28 859
Run 2	483	3122	21 211	10 686	27 035
Run 3	484	3091	18 178	10 158	26 270
CPR-AMG	478	2981	9764	8967	22 951

The simulation was run for 2520 days. The initial conditions of the reservoir are shown in Fig. 11. The coarsening factors for the three directions were $5 \times 5 \times 3$, which resulted in a coarse grid of $36 \times 27 \times 9$, a total of 8748, cells.

5.2.1. Simulations without capillary pressure

The settings of the three runs chosen for this test case are shown in Table 5. The results obtained with Run 1 and Run 2 suggested that an extra iteration for each smoothing step could help limiting the number of linear iterations, which was then considered for Run 3.

Results for the three runs are shown in Table 6. The best performance is obtained by introducing an extra pre- and post-smoothing iteration as this allows to reduce the number of linear iterations. The improved quality of the pressure solution also affects the number of nonlinear iterations. In fact, the difference in the number of nonlinear iteration between Run 1 and the reference one is much higher than the one observed with the previous model. This results in a higher CPU time for the overall simulation. A promising finding is that simulation times for all three runs are comparable with that of CPR-AMG.

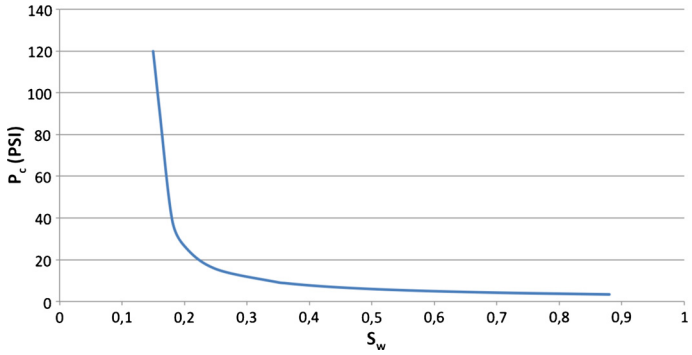

Fig. 12. Capillary pressure curve considered for the case Brill.

Table 7
Brill model with capillary pressure: settings. Differences can be seen in the smoothers and in the solver used on the coarse scale pressure system.

Runs	Pre-smoothing	Post-smoothing	Coarse solver
Run 1	GS	GS	AMG
Run 2	GS	GS	GMRES-AMG
Run 3	2xGS	2xGS	GMRES-AMG

Table 8
Brill model with capillary pressure: the table shows the total numbers of nonlinear and of linear iterations and the total and the linear solver CPU time of each run.

Runs	Timesteps	Iteration count		CPU time (s)	
		Nonlinear	Linear	Linear solver	Total
Run 1	340	1596	11 863	5739	14 213
Run 2	341	1608	12 234	5863	14 348
Run 3	341	1610	10 679	5745	14 454
CPR-AMG	342	1610	5749	5045	12 750

5.2.2. Simulations with capillary pressure

The capillary pressure curve as shown in Fig. 12 was then added to the Brill model. As for the previous model, this was done to test the CPR-MS solver on a test case with a stronger coupling between the variables.

Table 7 summarizes the settings of the three runs that are considered for the Brill model with capillary pressure. Once again, different number of iterations of the smoothers and different solution strategies on the coarse scale pressure system were used.

The results for this test case are shown in Table 8. The performance of the CPR-MS and CPR-AMG for this challenging test case is quite comparable, though the CPR-MS CPU time is about 11.5% more than that of CPR-AMG for the best scenario which is Run 1. Note that with adaptivity of basis functions update, and space–time adaptive employment of iterations within AMS framework [6,20] for FIM systems, which is the topic of our ongoing research. As observed for the previous test cases, the number of linear iterations for CPR-MS is typically more than CPR-AMG which is consistent with the literature [18,19].

6. Conclusion

The first multiscale method for fully implicit simulation of multiphase multicomponent flows in heterogeneous three-dimensional media with capillary and gravitational effects was developed in this paper. The CPR decoupling operator is used to extract the pressure system to which an MS method is eventually applied. Following the steps of CPR preconditioning, after having solved the pressure system, a second stage preconditioner (i.e., ILU(0)) is used as the second stage solver for FIM system.

MS restriction and prolongation operators were obtained by solving basis functions using IMPES formulation. A study of the best formulation for basis functions is the subject of ongoing research.

The results for the presented test cases, which were challenging for a sequential simulator, showed promising application for multiscale methods for FIM simulations. Compared with AMG solvers, MS methods benefit from aggressive coarsening ratios with accurate prolongation operators on the basis of locally computed basis functions. Further studies are required to exploit full adaptivity of the multiscale methods along with conservative property of MSFV into the FIM system. Both of

Table 9
Component molar fractions for black oil model. Note that $\rho_{j,ST}$ is the density of phase j at stock tank conditions [31,7].

$x_{oo} = \frac{\rho_{o,ST}}{\rho_{o,ST} + R_s \rho_{g,ST}}$	$x_{wo} = 0$	$x_{go} = 1 - x_{oo}$
$x_{ow} = 0$	$x_{ww} = 1$	$x_{gw} = 0$
$x_{og} = 0$	$x_{wg} = 0$	$x_{gg} = 1$

Table 10
Phase properties used for simulations presented in this paper.

S_w dependent			S_o dependent			S_g dependent	
S_w	k_{rw}	p_{cow} [psi]	S_o	k_{row}	k_{rog}	S_g	k_{rog}
0.15	0.0	120	0.12	0.00	0.0	0.00	0.0
0.16	0.0	91.47231262	0.29	0.0016	0.08333	0.04	0.0
0.18	0.0	39.28921117	0.40	0.0162	0.16667	0.10	0.02
0.20	0.0001	26.5228644	0.54	0.0950	0.25	0.20	0.1
0.35	0.0003	9.130558739	0.60	0.1714	0.33333	0.30	0.24
0.36	0.0103	8.794231502	0.62	0.4350	0.41667	0.40	0.34
0.37	0.0222	8.485097318	0.63	0.5680	0.5	0.50	0.42
0.38	0.0359	8.199865113	0.64	0.7005	0.58333	0.60	0.5
0.40	0.0695	7.690440048	0.65	0.8302	0.66667	0.70	0.813
0.46	0.1049	6.517609798	0.80	0.9788	0.75	0.85	1.0
0.60	0.2104	4.893140943	0.82	0.9916	0.83333		
0.71	0.3187	4.135515361	0.84	0.9995	0.91667		
0.88	0.4900	3.372596478	0.85	1.0	1.0		

Table 11
Phase thermodynamics equilibrium properties of oil and gas used for simulations of this paper. For water, $C_w = 10^{-6}$ [1/psi], $\mu_w = 0.96$ [cp], and $B_w = 1.0034$ are used.

Oil PVT				Gas PVT		
R_s	p_{bub} [psi]	B_o	μ_o [cp]	p [psi]	B_g	μ_g [cp]
0.0	14.7	1.062	1.04	14.696	166.6	1.0
0.371	1114.7	1.295	1.037	1114.7	3.197	1.0
0.636	3314.7	1.435	1.035	3314.7	1.614	1.0
0.93	5514.7	1.565	1.03	5514.7	1.080	1.0
1.27	8814.7	1.695	1.02	8814.7	0.811	1.0
	15014.7	1.579	1.04	15014.7	0.386	1.0

these additions are the topic of our ongoing research. With the CPR-MS development, multiscale method are now applicable to a wider range of problems with strong coupling terms.

Acknowledgements

This work was sponsored by Chevron/Schlumberger Intersect Technology Alliance, Schlumberger Abingdon Technology Centre, and Schlumberger Petroleum Services CV. Authors also thank the INTERSECT simulator and Research & Prototyping teams for the fruitful discussions during the development of CPR-MS method.

Appendix A

Black oil simulations can be obtained by using the information provided in Table 9.

The phase properties used for the simulations are presented in Table 10.

Thermodynamics equilibrium data of Table 11 has been used in order to obtain the simulations of this paper. Note that B_j stands for formation volume factor of j, the ratio of volumes at reservoir condition to stock tank condition [31].

References

[1] P. Jenny, S.H. Lee, H.A. Tchelepi, Multi-scale finite-volume method for elliptic problems in subsurface flow simulation, J. Comput. Phys. 187 (2003) 47–67.
[2] T.Y. Hou, X.-H. Wu, A multiscale finite element method for elliptic problems in composite materials and porous media, J. Comput. Phys. 134 (1997) 169–189.
[3] P. Jenny, S.H. Lee, H.A. Tchelepi, Adaptive fully implicit multi-scale finite-volume method for multi-phase flow and transport in heterogeneous porous media, J. Comput. Phys. 217 (2006) 627–641.
[4] Y. Efendiev, T.Y. Hou, Multiscale Finite Element Methods: Theory and Applications, Springer, 2009.
[5] H. Hajibeygi, P. Jenny, Multiscale finite-volume method for parabolic problems arising from compressible multiphase flow in porous media, J. Comput. Phys. 228 (2009) 5129–5147.

[6] H. Hajibeygi, P. Jenny, Adaptive iterative multiscale finite volume method, J. Comput. Phys. 230 (3) (2011) 628–643.
[7] H. Hajibeygi, H.A. Tchelepi, Compositional multiscale finite-volume formulation, SPE J. 19 (2) (2014) 316–326.
[8] H. Hajibeygi, D. Karvounis, P. Jenny, A hierarchical fracture model for the iterative multiscale finite volume method, J. Comput. Phys. 230 (24) (2011) 8729–8743.
[9] H. Zhou, H.A. Tchelepi, Operator based multiscale method for compressible flow, in: SPE Reservoir Simulation Symposium, Houston, TX, USA, 2007, SPE paper 106254.
[10] S.H. Lee, C. Wolfsteiner, H.A. Tchelepi, Multiscale finite-volume formulation for multiphase flow in porous media: black oil formulation of compressible, three-phase flow with gravity, Comput. Geosci. 12 (3) (2008) 351–366.
[11] C. Wolfsteiner, S.H. Lee, H.A. Tchelepi, Well modeling in the multiscale finite volume method for subsurface flow simulation, Multiscale Model. Simul. 5 (3) (2006) 900–917.
[12] P. Jenny, I. Lunati, Modeling complex wells with the multi-scale finite volume method, J. Comput. Phys. 228 (2009) 687–702.
[13] H. Zhou, S.H. Lee, H.A. Tchelepi, Multiscale finite-volume formulation for saturation equations, SPE J. 17 (1) (2011) 198–211.
[14] D. Cortinovis, Patrick Jenny, Iterative Galerkin-enriched multiscale finite-volume method, J. Comput. Phys. 277 (2014) 248–267.
[15] O. Moyner, K.A. Lie, The multiscale finite-volume method on stratigraphic grids, SPE J. 19 (5) (2014), http://dx.doi.org/10.2118/163649-PA.
[16] H. Hajibeygi, G. Bonfigli, M.A. Hesse, P. Jenny, Iterative multiscale finite-volume method, J. Comput. Phys. 227 (2008) 8604–8621.
[17] H. Zhou, H.A. Tchelepi, Two-stage algebraic multiscale linear solver for highly heterogeneous reservoir models, SPE J. 17 (2) (2012) 523–539.
[18] Y. Wang, H. Hajibeygi, H.A. Tchelepi, Algebraic multiscale linear solver for heterogeneous elliptic problems, J. Comput. Phys. 259 (2014) 284–303.
[19] M. Tene, H. Hajibeygi, Y. Wang, H.A. Tchelepi, Compressible algebraic multiscale solver (CAMS), in: Proceedings of the 14th European Conference on the Mathematics of Oil Recovery (ECMOR), Catania, Sicily, Italy, 2014.
[20] H. Hajibeygi, S.H. Lee, I. Lunati, Accurate and efficient simulation of multiphase flow in a heterogeneous reservoir by using error estimate and control in the multiscale finite-volume framework, SPE J. 17 (4) (2012) 1071–1083.
[21] A.G. Spillette, J.G. Hillestad, H.L. Stone, A high-stability sequential solution approach to reservoir simulation, SPE J. (1973), http://dx.doi.org/10.2118/4542-MS, SPE-4542-MS.
[22] K.H. Coats, W.D. George Chieh Chu, B.E. Marcum, Three-dimensional simulation of steamflooding, SPE J. 14 (6) (1974) 573–592.
[23] J. Moortgat, A. Firoozabadi, Three-phase compositional modeling with capillarity in heterogeneous and fractured media, SPE J. 18 (6) (2013), http://dx.doi.org/10.2118/159777-PA.
[24] J. Kou, S. Sun, Analysis of a combined mixed finite element and discontinuous Galerkin method for incompressible two-phase flow in porous media, Math. Methods Appl. Sci. 37 (2014) 962–982.
[25] R. Younis, Advances in modern computational methods for nonlinear problems: a generic efficient automatic differentiation framework, and nonlinear solvers that converge all the time, PhD thesis, Stanford University, USA, 2009.
[26] H. Cao, Development of techniques for general purpose simulation, PhD thesis, Stanford University, USA, 2002.
[27] J.R. Wallis, R.P. Kendall, T.E. Little, J.S. Nolen, Constrained residual acceleration of conjugate residual methods, in: SPE Reservoir Simulation Symposium, 1985.
[28] H. Cao, H.A. Tchelepi, J.R. Wallis, H. Yardumian, Constrained residual acceleration of conjugate residual methods, in: SPE Annual Technical Conference and Exhibition, Dallas, Texas, USA, 2005, SPE paper 96809.
[29] U. Trottenberg, C.W. Oosterlee, A. Schueller, Multigrid, Elsevier Academic Press, 2001.
[30] F.M. Orr, Theory of Gas Injection Processes, Tie-Line Publication, Denmark, 2007.
[31] K. Aziz, A. Settari, Petroleum Reservoir Simulation, Blitzprint Ltd., Calgary, Alberta, 2002.
[32] J.R. Wallis, Incomplete Gaussian elimination as a preconditioning for generalized conjugate gradient acceleration, in: SPE Reservoir Simulation Symposium, 1983.
[33] R.E. Bank, T.F. Chan, W.M. Coughran Jr., R.K. Smith, The alternate-block-factorization procedure for systems of partial differential equations, BIT Numer. Math. 29 (1989) 938–954.
[34] K. Stuben, T. Clees, H. Klie, B. Lu, M.F. Wheeler, Algebraic multigrid methods (AMG) for the efficient solution of fully implicit formulations in reservoir simulation, in: 2007 Reservoir Simulation Symposium, 2007, SPE paper 105832.
[35] J. Wallis, H.A. Tchelepi, H. Cao, Apparatus, method and system for improved reservoir simulation using a multiplicative overlapping Schwarz preconditioning for adaptive implicit linear systems, USA patent 007516056B2, 2009.
[36] Y. Saad, M.H. Schultz, GMRES: a generalized minimal residual algorithm for solving nonsymmetric linear systems, SIAM J. Sci. Stat. Comput. 7 (3) (1986) 856–869.
[37] Y. Saad, A flexible inner–outer preconditioned GMRES algorithm, SIAM J. Sci. Stat. Comput. 14 (2) (1993) 461–469.
[38] Y. Saad, Iterative Methods for Sparse Linear Systems, SIAM, Philadelphia, USA, 2003.
[39] L.S.K. Fung, A.H. Dogru, Parallel unstructured solver methods for complex giant reservoir simulation, in: SPE Reservoir Simulation Symposium, Houston, Texas, USA, 2007, SPE paper 106237.
[40] J.W. Watts, A total velocity sequential preconditioner for solving implicit reservoir simulation matrix equations, in: SPE Reservoir Simulation Symposium, Houston, Texas, USA, 1999, SPE paper 51909.
[41] A.A. Lukyanov, H. Hajibeygi, J. Natvig, K. Bratvedt, A multilevel Galerkin and non-Galerkin, conditionally and unconditionally monotone constrained pressure residual multiscale methods, US patent, Docket No. IS14.8805, 2014.
[42] J.E. Killough, Ninth SPE comparative solution project: a reexamination of black-oil simulation, in: SPE Symposium on Reservoir Simulation, San Antonio, Texas, February 1995, SPE-29110-MS.
[43] Intersect technical and reference manual v. 2014.1, 2014.